

Swimming mode determines how well mesoscale swimmers shield their odor in turbulence

Martin James,^{1,*} Francesco Viola,² and Agnese Seminara^{1,†}

¹*Machine Learning Genoa Center (MaLGA) & Department of Civil, Chemical and Environmental Engineering, University of Genoa, Genoa, Italy*

²*Gran Sasso Science Institute, L'Aquila, Italy*

(Dated: January 1, 2025)

Marine organisms manipulate their surrounding flow through their swimming dynamics, which affects the transport of their own odor cues. We demonstrate by direct numerical simulations how a group of mesoscale swimmers immersed in a turbulent flow alters the shape of the odor plume they release in the water. Odor mixing is enhanced by increased velocity fluctuations and a swimmer-induced flow circulation which widens the odor plume at close range while speeding up dilution of the chemical trace. Beyond a short-range increase in the likelihood of being detected, swimming considerably reduces detections with effects that can persist at distances of the order of ten times the size of the group or more. We find that puller-like swimmers are more effective at olfactory shielding than pusher-like swimmers. We trace this difference back to the dynamics at the swimmer location, which tends to trap odor at the source for pushers and to dilute it for pullers. Olfactory shielding is robust to changes in the conditions, and is more pronounced for weak turbulent Reynolds numbers and large swimmer Reynolds numbers. Our results suggest that olfactory shielding may play a role in the emergence of different swimming modalities by marine organisms.

I. INTRODUCTION

Groups of swimming organisms are a major target for large predators who employ multiple sensory cues to track them down. In particular, swimmers give out their whereabouts by shedding odor, which is carried downstream of the group by water flow and can be detected by predators even from large distances (see, e.g., [1, 2] and references therein). As odor is transported away from the group, it undergoes turbulent mixing, which merges odor-laden and odor-free water. Mixing will ultimately erase their chemical trace as odor gets diluted below the threshold of detection of potential predators. The act of swimming in itself enhances turbulent mixing by actively manipulating the surrounding flow in a process known as biomixing, as documented by laboratory and numerical studies (see, e.g., [3] and references therein). Biomixing may even affect the global ocean circulation, although its quantification is challenging and hotly debated [4, 5]. As a direct consequence of the documented enhanced mixing one expects that odor will dilute more efficiently, speeding up the elimination of the swimmers' own odor trace, as previously hypothesized for filter feeding by sessile organisms [6, 7]. Given the fascinating diversity of species in the ocean, one naturally wonders whether specific ways of swimming may be more efficient than others at this mechanism, that we refer to as olfactory shielding.

Swimming organisms leverage a diversity of self-propulsion mechanisms, e.g. beating or rotating appendages like cilia or flagella or propagating shape deformations [8, 9]. Mesoscale swimmers such as copepods,

amphipods and other small crustaceans form an important part of the marine ecosystem. They serve as pivotal food sources for larger marine species and play an important role in marine ecology [10]. Such species are often found in large groups [11] and inhabit regions of mild-to-moderate turbulence [8, 12, 13]. At the micro- and meso-scales, swimmers can exhibit pusher or puller dynamics, depending on whether they generate thrust at their rear or front during specific swimming modes [14, 15]. The hydrodynamic interactions by pushers and pullers generate distinct patterns in their surrounding water flow, both individually [15–17] as well as in groups [18, 19]. But whether and how mesoscale pushers *vs* pullers are more or less efficient at olfactory shielding remains to be understood.

In this article, we provide a detailed analysis of the coupling of mechanical and chemical signals from mesoscale swimmers in turbulent flows. We conduct high-resolution direct numerical simulations using a model system of a collection of point swimmers in an open channel turbulent flow. We show that groups of swimmers enhance mixing, and puller-like swimmers are more efficient than pusher-like swimmers at olfactory shielding. We demonstrate that this effect is stronger for large swimmer Reynolds numbers and low flow Reynolds numbers, suggesting that olfactory shielding may contribute selective pressure on mesoscale swimmers in the ocean.

II. MODELING AND METHODOLOGY

We consider a collection of mesoscale swimmers moving at a uniform, constant velocity, embedded in an open channel flow. The fluid flow is modeled through direct numerical simulation of the incompressible Navier-Stokes equation

* martin.james@edu.unige.it

† agnese.seminara@unige.it

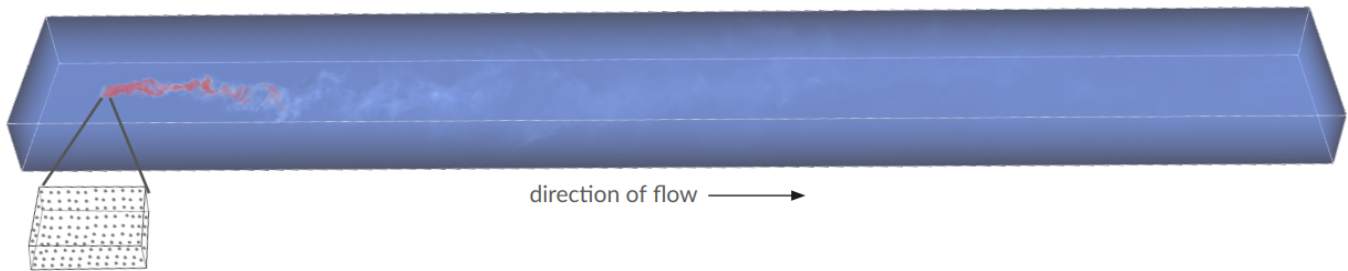


FIG. 1. A snapshot of the odor field emitted by the swimmers. The swimmers are placed in a cuboidal box of dimension $100\eta \times 100\eta \times 25\eta$ near the inlet, as shown in the inset. The simulation box has a dimension of $8000\eta \times 1000\eta \times 400\eta$.

No.	Re_τ	Re_s
1	560	50
2	560	25
3	560	10
4	685	50
5	395	50

TABLE I. List of environments with the corresponding friction Reynolds numbers Re_τ of the channel flow and the swimmer Reynolds numbers Re_s .

$$\rho \left(\frac{\partial \mathbf{u}}{\partial t} + \mathbf{u} \cdot \nabla \mathbf{u} \right) = -\nabla P + \mu \nabla^2 \mathbf{u} + \mathbf{f} + \mathbf{f}_p; \quad (1)$$

$$\nabla \cdot \mathbf{u} = 0.$$

Here, \mathbf{u} is the fluid velocity field, P is the pressure, ρ is the fluid density, μ is the dynamic viscosity and \mathbf{f}_p is the forcing due to the swimmer dynamics. We solve equation (1) using a second-order central finite-difference scheme on a staggered grid [20].

The channel is forced with a constant pressure gradient \mathbf{f} [21]. The boundary conditions for the channel flow are as follows: a fixed velocity on the bottom boundary (to represent the appropriate swimming velocity of the swimmers, as the simulations are carried out in the reference frame of the swimmers), free slip on the top boundary ($u_z = 0, \partial_z u_x = \partial_z u_y = 0$) and periodic in the other directions. We simulate three different fluid friction Reynolds numbers $Re_\tau = u_\tau H / \nu$, where u_τ is the shear velocity, H is the channel height and ν is the kinematic viscosity ($\nu = \mu / \rho$), as shown in Table I. We choose Environment 1 in Table I as our base environment and all units are normalized by using the Kolmogorov scales in this simulation. The simulation box has a dimension of $8000\eta \times 1000\eta \times 400\eta$.

The odor field is modeled using an advection-diffusion equation.

$$\frac{\partial c}{\partial t} + \mathbf{u} \cdot \nabla c = D \nabla^2 c + s. \quad (2)$$

Here c is odor concentration, D is the diffusivity and s is the odor source. We assume perfect adsorption on the

bottom boundary ($c = 0$), no flux at the top boundary ($\partial_z c = 0$) and outflow conditions at the other boundaries. We use a constant source term at the position of the swimmers. For our simulations, we use Schmidt number $Sc = 1$. Although Sc in water is typically higher than this, we anticipate a weak dependence on Sc since we are interested in large-scale statistics [22, 23].

To model the forcing \mathbf{f}_p due to the swimmers, note that the swimmers move at a constant velocity thus the net force on them is zero. The flow field due to neutrally buoyant micro and mesoscale swimmers can be approximated by a force dipole [24–26]. Further addition of torque dipoles combined with rigid boundary conditions can effectively capture swimmers moving at even higher Re [27]. However, since our swimmers are of the order of the Kolmogorov scale and move at relatively low Re , we model our swimmers using a force dipole approximation. Each swimmer is modeled as a force dipole oriented along the streamwise direction $F(\delta(\mathbf{x} + \mathbf{r}) - \delta(\mathbf{x} - \mathbf{r}))\hat{\mathbf{x}}$, where r is half the length of the swimmer and F is the magnitude of the forcing. The orientation of the force dipole determines whether the swimmer is pusher-like or puller-like. When the forcing points outwards relative to the swimmer’s axis, the swimmer “pushes” the fluid away and is a pusher-like swimmer whereas, when it points inwards, it “pulls” the fluid in, thus modeling a puller-like swimmer [15]. The magnitude of F is computed based on the experimental results for the drag force at intermediate Reynolds numbers [28] (also see Eq. S1 in the Supporting Information). The swimmers are placed in a cuboidal box of dimension $100\eta \times 100\eta \times 25\eta$ close to the inlet with a total of $10 \times 20 \times 5$ swimmers along the streamwise, spanwise and wall-normal directions respectively.

We consider three different Reynolds numbers for the swimmers $Re_s = u_s D / \nu$, where u_s is the magnitude of the swimming velocity and D is the diameter, as shown in Table I. To achieve different swimmer Reynolds numbers, the velocities of the swimmers are adjusted by modifying the fluid velocity boundary condition applied on the bottom wall, with all other parameters held constant. The simulations are conducted in the reference frame of the swimmers. All simulations are run until at least $T = 4 \times 10^3 \tau_\eta$ to reach a statistically steady state before

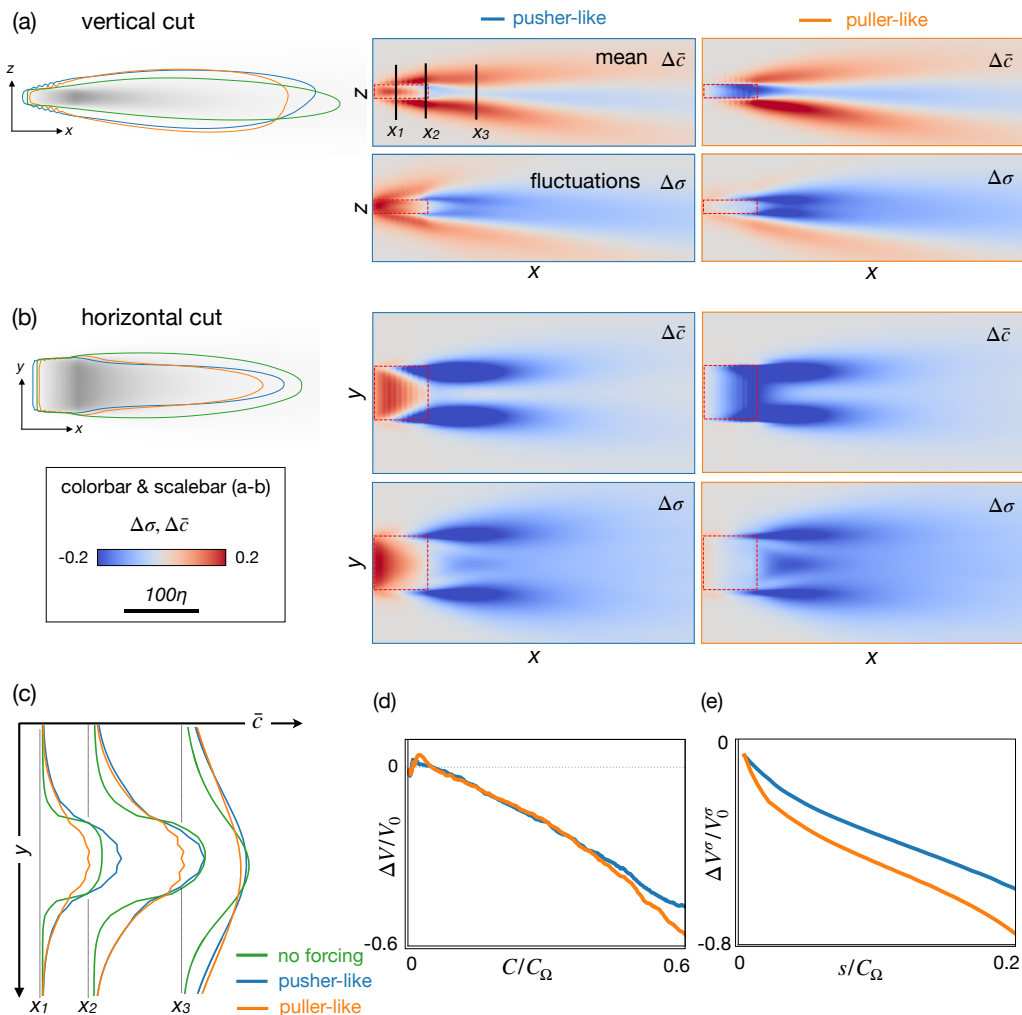


FIG. 2. Statistics of the mean odor field. The contour plots show how the range of the mean odor field varies between pusher-like, puller-like and neutral swimmers for vertical and horizontal mid-plane cross-sections. (a) Vertical cross-sections of the mean odor differential $\Delta\bar{c}(\mathbf{x})$ for pusher-like swimmers and puller-like swimmers and the corresponding odor standard deviation differential $\Delta\sigma(\mathbf{x})$. The region containing the swimmers is marked by a red box. (b) The corresponding figures for the horizontal cross-section. (c) Odor profiles at different distances from the swimmers' location. (d) Shielding intensities of the mean odor field $\Delta V(C)/V_0(C)$. (e) Shielding intensity of the odor fluctuations $\Delta V^\sigma(s)/V_0^\sigma(s)$ for pusher-like and puller-like swimmers, showing that the swimming dynamics dampens large fluctuations.

the results are evaluated.

The list of environments is given in Table I. All figures correspond to the base environment (Simulation 1 in Table I) unless otherwise mentioned. For each of these environments, we conduct three distinct simulations: In the first two, we incorporate the dynamics of the swimmers by accounting for the forcing imposed by the swimmers on the fluid – pusher-like or puller-like; then we remove this forcing, providing a baseline against which to measure the swimmers' effects. The simulation setup is shown in Fig. 1, illustrating a typical case of odor dispersion in a channel flow.

III. RESULTS

To determine whether swimmers' dynamics leave their signatures in the odor distribution over long time-scales, we begin our analysis by examining the effect of hydrodynamic interactions on the mean and standard deviation of the odor field (Fig. 2). Since the odor distribution is inhomogeneous and statistically stationary, we approximate the ensemble average of the mean and standard deviation of the odor field with temporal averages:

$$\bar{c}(\mathbf{x}) = \langle c(\mathbf{x}, t) \rangle \quad (3)$$

$$\sigma(\mathbf{x}) = \langle (c(\mathbf{x}, t) - \bar{c}(\mathbf{x}, t))^2 \rangle^{\frac{1}{2}}.$$

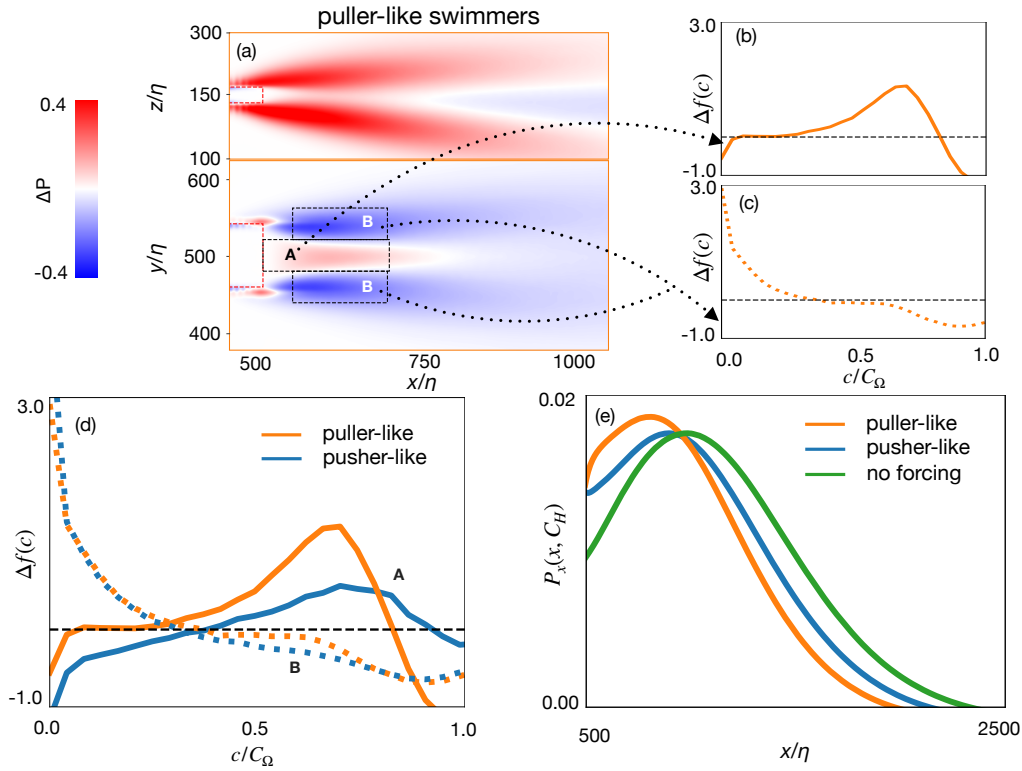


FIG. 3. The effect of swimming dynamics on the detection probability. (a) $\Delta P(\mathbf{x}; C_H)$ for puller-like swimmers. (b) and (c) Odor pdf differential $\Delta f(c)$ in regions A and B, respectively, for puller-like swimmers. (d) Odor pdf differential $\Delta f(c)$ for both types of swimmers; statistics in regions A and B are represented with solid and dotted lines respectively. (e) Detection probability $P_x(x; C_H)$ as a function of stream-wise distance, averaged along y and z . The x -axis starts at $x = 500$, where the group of swimmers ends. At long distances $x \gtrsim 700\eta$ the detection probability is reduced due to the swimming dynamics. Shielding persists up to $x \sim 2500\eta$

To account for the effect of the swimmers, we now define differential quantities by comparison with the baseline simulation that ignores the presence of the swimmers:

$$\begin{aligned} \Delta \bar{c}_s(\mathbf{x}) &= [\bar{c}_s(\mathbf{x}) - \bar{c}_0(\mathbf{x})]/C_\Omega \\ \Delta \sigma_s(\mathbf{x}) &= [\sigma_s(\mathbf{x}) - \sigma_0(\mathbf{x})]/C_\Omega, \end{aligned} \quad (4)$$

where the subscript s stands for swimmers (either pusher-like or puller-like), and the subscript 0 represents the baseline simulation. Mean and fluctuations are normalized by $C_\Omega = \max(\bar{c}_0)$, which occurs within the volume Ω containing the swimmers.

Swimmer dynamics strongly affect the odor mean and fluctuations, with deviations up to 20% of C_Ω (Fig. 2 (a-b)). This effect varies in different regions of space, as swimmers are clustered together. Within the region Ω that contains the swimmers, pusher-like and puller-like dynamics affect odor in opposite ways. Pusher-like swimmers *concentrate* the odor average within Ω and *increase* odor fluctuations, whereas puller-like swimmers *dilute* the odor average and *decrease* its fluctuations (Fig. 2 (a-b)). Outside of Ω , both swimming modalities have the same qualitative effects, which however differ quantitatively and vary in space. Within the wake, both

swimmers lead to a decrease in odor mean and fluctuations; outside of the wake, in the wall-normal direction – i.e. vertical cut, Fig. 2 (a), above and below the wake – swimmers increase odor mean and fluctuations; whereas in the spanwise direction – i.e. horizontal cut Fig. 2 (b), swimmers decrease odor mean and fluctuations.

To quantify the overall effect of swimmers in the entire volume, we define the volumes $V(C)$ where the mean odor concentration exceeds C and $V^\sigma(s)$ where the fluctuations exceed s :

$$\begin{aligned} V_s(C) &= \int H(\bar{c}_s(\mathbf{x}) - C) d\mathbf{x}, \\ V_s^\sigma(s) &= \int H(\sigma_s(\mathbf{x}) - s) d\mathbf{x}, \end{aligned}$$

where $H(x)$ is the Heaviside step function and integration is extended to the entire domain. We define the shielding efficiency as the decrease in the volumes defined above:

$$\begin{aligned} \Delta V_s(C) &= V_s(C) - V_0(C), \\ \Delta V_s^\sigma(s) &= V_s^\sigma(C) - V_0^\sigma(s). \end{aligned}$$

When $C \approx 0$, swimming dynamics has little to no effect (or even a weak negative effect) in shielding the mean

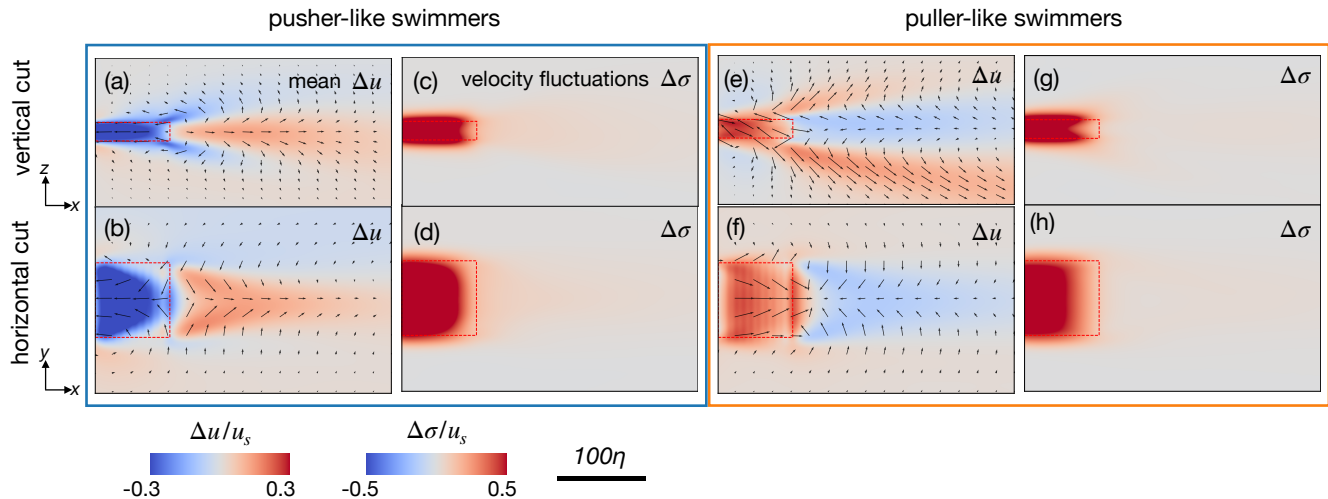


FIG. 4. Effect of swimming dynamics on fluid velocity. Difference in the mean streamwise velocity due to the swimmers’ dynamics, normalized with the swimmer speed for (a,b) pusher-like and (e,f) puller-like swimmers. Difference in the standard deviation of the cross-stream velocity fluctuations for (c,d) pusher-like and (g,h) puller-like swimmers.

odor, with puller-like swimmers performing slightly worse than pusher-like ones (Fig. 2 (d)). As C is increased, $\Delta V(C) < 0$ thus both types of swimmers decrease the total volume where the average concentration is above the threshold. For a threshold of $C/C_\Omega = 0.5$, pullers shrink $V(C)$ by 50%, while pushers shrink $V(C)$ by 45%. Similarly, shielding efficiency for odor fluctuations (Fig. 2 (e)) shows that regions with extreme fluctuations are significantly reduced when the swimmer dynamics are taken into account. Interestingly, puller-like swimmers exhibit better shielding of both mean and fluctuations, which may reduce the chances of detection.

We hypothesize that the damping of odor mean and fluctuations is a consequence of enhanced mixing due to the presence of the swimmers. To corroborate this intuition, we examine the full probability distribution of the odor field:

$$f(c, \mathbf{x}) = \langle \delta(c(\mathbf{x}, t) - c) \rangle, \quad (5)$$

where $f(c, \mathbf{x})$ represents the probability density of the odor field $c(\mathbf{x}, t)$ taking the value c at a specific point \mathbf{x} . Here, $\delta(\cdot)$ is the Dirac delta function and the angular bracket denotes the expectation. The right tail of $f(c, \mathbf{x})$ defines the probability of detecting odor at a threshold C through:

$$P(\mathbf{x}, C) = \int_C^\infty f(c, \mathbf{x}) dc. \quad (6)$$

To quantify shielding we focus on the variation of P due to the swimmers relative to the baseline simulation: $\Delta P_s(\mathbf{x}, C) = P_s(\mathbf{x}, C) - P_0(\mathbf{x}, C)$. C is often hard to measure as it depends on a complex interaction between environmental conditions, the chemical identity of the odor and the predator. We exemplify results

using two thresholds, “high” $C_H = 0.1 C_\Omega$ and “low” $C_L = 0.01 C_\Omega$.

The probability of detection generally increases above and below the swimmers, and it decreases left and right (vertical and horizontal cross cut, Fig. 3 (a-b)). Within the horizontal cut, a further distinction needs to be made between a thin core region in the immediate downstream of the group (region A in Fig. 3 (a)), where swimmers *increase* their detection probability, and regions outside this thin core, both further downstream and at the outer edges of the wake (region B in the Figure), where swimmers *decrease* their detection probability. The same qualitative pattern holds for lower thresholds, with region A expanding further and further downstream as the threshold is decreased (see Fig. S3), consistent with the results illustrated for the mean (Fig. 2 (d-e)). For pusher-like swimmers, all patterns are qualitatively preserved, although the intensity of shielding differs (see Fig. S3).

Unintuitively, the two swimmer types have opposite effects at the odor source, yet they both shrink their own detection probability at large enough distances from the group. This is best summarized by monitoring the probability of detection as a function of distance x downstream of the swimmers:

$$P_x(x, C) = \frac{1}{L_z L_y} \int_0^{L_z} \int_0^{L_y} P(\mathbf{x}, C) dy dz. \quad (7)$$

The group increases their probability of detection at close range, i.e. within $\sim 200\eta$ from the end of the group, about twice the length of the group. At longer range the group decrease their detection probability (Fig. 3 (e)). Importantly, shielding persists up to $\sim 2000\eta$, i.e. 20 times the length of the group. To reconcile this unintuitive mismatch, we analyze the full probability density function within regions A and B and compare the simulations with

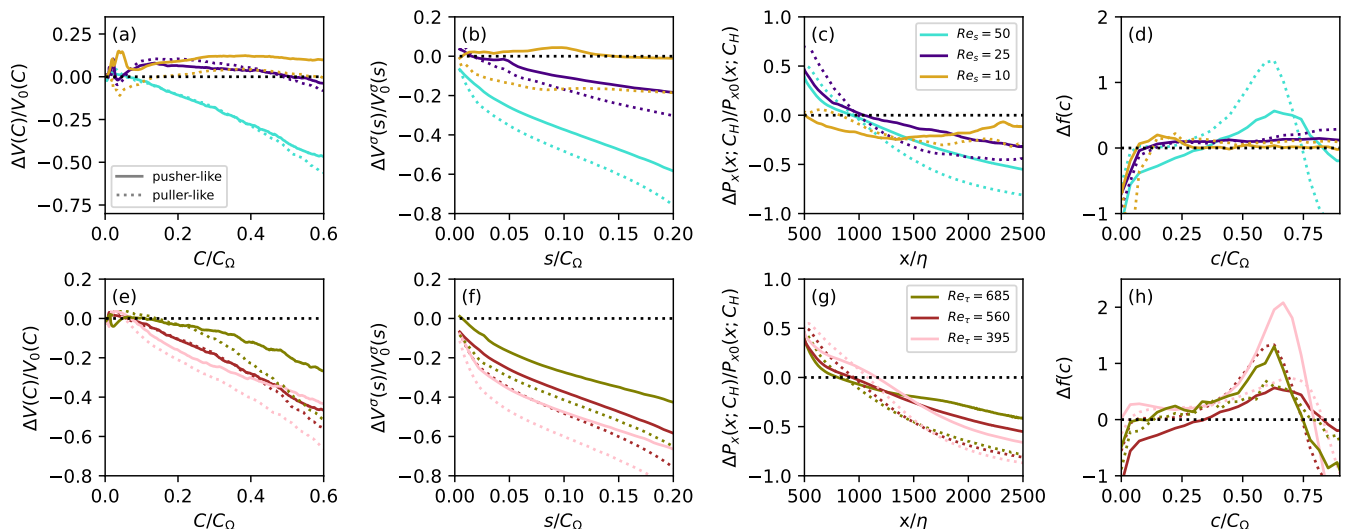


FIG. 5. (a) Shielding of odor mean $\Delta V(C)/V_0(C)$ as a function of normalized threshold C/C_Ω , (b) shielding of odor fluctuations $\Delta V^\sigma(s)/V_0^\sigma(s)$ as a function of normalized threshold s/C_Ω , (c) normalized detection probability differential $\Delta P_x(x; C_H)/P_{x0}(x; C_H)$ as a function of the streamwise distance from the swimmers and (d) odor pdf differential $\Delta f(c; \Omega_A/B)$. Colors represent different swimmer Reynolds numbers (a-d) or different turbulent Reynolds numbers (e-h). Pusher-like and puller-like swimmers are represented by solid and dotted lines respectively.

and without swimmers $\Delta f_s(c, \mathbf{x}) = f_s(c, \mathbf{x}) - f_0(c, \mathbf{x})$. In region A the swimmer dynamics dampen both extremes of the odor distribution (Fig. 3 (b)). This is a signature of increased mixing, which homogenizes the odor field towards its mean concentration. In region B the swimmer dynamics dilutes the odor, presumably by spreading it in a larger region further outward (Fig. 3 (c)). Pusher-like swimmers behave qualitatively similarly (Fig. 3 (d)). These signatures of enhanced mixing suggest that the velocity fluctuations due to the swimmer dynamics play a major role in odor transport.

To understand the origin of shielding and corroborate the role of increased mixing, we examine how swimmers affect their surrounding flow field (Fig. 4). First, there is a marked difference in how swimmers affect the mean flow at their own location. Pusher-like swimmers slow down the mean flow, whereas puller-like swimmers accelerate the mean flow (Fig. 4 (a-b)), consistent with the results on the motility of inertial pusher-like and puller-like squirmers [29]. By odor conservation, a slow down of the mean flow by the pushers will tend to concentrate the odor within the source region Ω , whereas the acceleration of the mean flow by the pullers will tend to dilute it.

Downstream of the source, the mean flow pushes the water up and down vertically (Fig. 4 (a,b)) and draws it inward laterally in the horizontal plane (Fig. 4 (e,f)). As a result, odor spreads vertically and shrinks laterally, and the probability of detection increases outside of the wake in the vertical plane, whereas it decreases outside of the core region in the horizontal plane. Finally, increased mixing in the core region A (Fig. 3 (d)) is caused by increased fluctuations, which occur for both kinds of

swimmers (Fig. 4 (c-d,g-h)).

In summary: both swimmer types cause the odor plume to bulge vertically and shrink laterally, and also increase velocity fluctuations. As a consequence, swimmers speed up dilution of the odor downstream of their position thus shrinking the probability that a potential predator may detect them. However, pullers are more effective at olfactory shielding because they additionally *dilute* odor at the source, whereas pushers *trap* odor at the source. Note that our problem is anisotropic due to the presence of the wall and the arrangement of the swimmers within the group, as noticed by comparing odor patterns in the spanwise and wall-normal directions (Fig. 2 (a-b)). The anisotropy of the cuboid containing the swimmers is the dominant anisotropy. Indeed, when considering a cuboid with the same shape but rotated of 90 degrees, we obtain a similar pattern as the one visualized in Fig. 2, with the y - and z - axis swapped (see Supplementary Fig. S2). Small differences with respect to Fig. 2 can be attributed to the anisotropy of wall turbulence (see Supplementary Fig. S4). While the shape of the group of swimmers alters the quantitative aspects of the problem, odor shielding persists for the multiple swimmer aspect ratios that we present in the supporting information (see Fig. S1 and Fig. S2).

Having examined in detail odor shielding in the base environment, we now evaluate how the shielding changes as the Reynolds numbers of the swimmers and the advecting fluid are changed. At higher swimmer Reynolds numbers, the effect of forcing by the swimmers is expected to be more significant leading to an increase in shielding efficiency with Re_s . Our numerical experiments confirm this expectation (Fig. 5 (a-d)). Interestingly, at

lower swimmer Re of 10 and 25, the swimmers' dynamics have little effect on shielding the mean odor (Fig. 5 (a)). However, the fluctuations in the odor field do carry signatures of the swimming dynamics even at lower Re for puller-like swimmers and consequently affect detection probabilities (Fig. 5 (b-c)). To understand how the fluid Re affects shielding, we repeat our analysis for two more fluid Re . Our analysis indicates that the effect of odor shielding is more prominent at lower fluid Reynolds numbers (Fig. 5 (e-h)). What is critical, however, is that puller-like swimmers continue to outperform pusher-like swimmers in all three fluid Re considered in our analysis.

In this work, we demonstrate how the hydrodynamic fluctuations introduced by a collection of mesoscale swimmers interact with their own odor field in a turbulent flow. We focus on two prototypic swimmer

types, pusher-like and puller-like, and show that in both cases the hydrodynamic interactions effectively erase the group's odor trace downstream of the swimmers. Importantly, puller-type swimmers shield odor more efficiently than pusher-like swimmers. Moreover, the effect increases at relatively low turbulence and fast swimming, providing potentially relevant mechanisms for predator avoidance. Interestingly, filter-feeding organisms like clams have been experimentally shown to frantically increase their motion upon exposure to predator cues [6]. These observations have been linked to an active response of filter feeders that increase mixing thus erasing odor more effectively [7]. Whether and how olfactory shielding may drive the evolution of different locomotion strategies or the emergence of active responses in swimming organisms remains to be tested.

-
- [1] D.R. Webster and M.J. Weissburg. The hydrodynamics of chemical cues among aquatic organisms. *Annu. Rev. Fluid Mech.*, 41:73–90, 2009.
- [2] G. Reddy, V.N. Murthy, and M. Vergassola. Olfactory sensing and navigation in turbulent environments. *Annu. Rev. Condens. Matter Phys.*, 13:191–213, 2022.
- [3] Eric Kunze. Biologically generated mixing in the ocean. *Annual review of marine science*, 11(1):215–226, 2019.
- [4] Kakani Katija and John O Dabiri. A viscosity-enhanced mechanism for biogenic ocean mixing. *Nature*, 460(7255):624–626, 2009.
- [5] André W Visser. Biomixing of the oceans? *Science*, 316(5826):838–839, 2007.
- [6] S.K. Delavan and D.R. Webster. Predator and flow influence on bivalve clam excurrent jet characteristics. *J. Exp. Mar. Biol. Ecol.*, 432:1–8, 2012.
- [7] A. Alvarez. Modeling the odor-landscape resulting from the pumping behavior of bivalve clams in the presence of predators. *J. Theor. Biol.*, 453:40–47, 2018.
- [8] J.S. Guasto, R. Rusconi, and R. Stocker. Fluid mechanics of planktonic microorganisms. *Annu. Rev. Fluid Mech.*, 44(1):373–400, 2012.
- [9] Theodore Yaotsu Wu. Fish swimming and bird/insect flight. *Annual review of fluid mechanics*, 43(1):25–58, 2011.
- [10] L. Ratnarajah, R. Abu-Alhaija, A. Atkinson, S. Batten, N.J. Bax, K.S. Bernard, G. Canonico, A. Cornils, J.D. Everett, M. Grigoratou, et al. Monitoring and modelling marine zooplankton in a changing climate. *Nat. Commun.*, 14(1):564, 2023.
- [11] G.R. Flierl and N.W. Woods. Copepod aggregations: influences of physics and collective behavior. *J. Stat. Phys.*, 158:665–698, 2015.
- [12] F.-G. Michalec, S. Souissi, and M. Holzner. Turbulence triggers vigorous swimming but hinders motion strategy in planktonic copepods. *J. R. Soc. Interface*, 12(106):20150158, 2015.
- [13] M. Omori and W.M. Hamner. Patchy distribution of zooplankton: behavior, population assessment and sampling problems. *Mar. Biol.*, 72:193–200, 1982.
- [14] N.B. Tack, S.O. Santos, B.J. Gemmill, and M.M. Wilhelmus. Ups and downs: Copepods reverse the near-body flow to cruise in the water column. *arXiv preprint arXiv:2404.04413*, 2024.
- [15] Eric Lauga and Thomas R Powers. The hydrodynamics of swimming microorganisms. *Reports on progress in physics*, 72(9):096601, 2009.
- [16] T. Kiørboe, H. Jiang, R.J. Gonçalves, L.T. Nielsen, and N. Wadhwa. Flow disturbances generated by feeding and swimming zooplankton. *Proc. Natl. Acad. Sci. U.S.A.*, 111(32):11738–11743, 2014.
- [17] L.A. van Duren and J.J. Videler. Escape from viscosity: the kinematics and hydrodynamics of copepod foraging and escape swimming. *J. Exp. Biol.*, 206(2):269–279, 2003.
- [18] Arne W Zantop and Holger Stark. Emergent collective dynamics of pusher and puller squirmer rods: swarming, clustering, and turbulence. *Soft Matter*, 18(33):6179–6191, 2022.
- [19] M Cavaio. Swarm of slender pusher and puller swimmers at finite reynolds numbers. *Physics of Fluids*, 34(2), 2022.
- [20] F. Viola, V. Meschini, and R. Verzicco. Fluid–structure–electrophysiology interaction (fsei) in the left-heart: a multi-way coupled computational model. *Eur. J. Mech. B Fluids*, 79:212–232, 2020.
- [21] M. Quadrio, B. Frohnappfel, and Y. Hasegawa. Does the choice of the forcing term affect flow statistics in dns of turbulent channel flow? *Eur. J. Mech. B Fluids*, 55:286–293, 2016.
- [22] N. Rigolli, N. Magnoli, L. Rosasco, and A. Seminara. Learning to predict target location with turbulent odor plumes. *Elife*, 11:e72196, 2022.
- [23] E. Selander, S.T. Fredriksson, and L. Arneborg. Chemical signaling in the turbulent ocean—hide and seek at the kolmogorov scale. *Fluids*, 5(2):54, 2020.
- [24] H. Jiang and T.R. Osborn. Hydrodynamics of copepods: a review. *Surv. Geophys.*, 25:339–370, 2004.
- [25] J. Drescher, K. Dunkel, L.H. Cisneros, S. Ganguly, and R.E. Goldstein. Fluid dynamics and noise in bacterial cell–cell and cell–surface scattering. *Proc. Natl. Acad. Sci. U.S.A.*, 108(27):10940–10945, 2011.
- [26] G.L. Wagner, W.R. Young, and E. Lauga. Mixing by microorganisms in stratified fluids. *J. Mar. Res.*, 72(2):47–

- 72, 2014.
- [27] B. Ventéjou, T. Métivet, A. Dupont, and P. Peyla. Universal scaling laws for a generic swimmer model. *arXiv preprint arXiv:2407.04511*, 2024.
 - [28] T.C. Granata and T.D. Dickey. The fluid mechanics of copepod feeding in a turbulent flow: a theoretical approach. *Prog. Oceanogr.*, 26(3):243–261, 1991.
 - [29] S Wang and A Ardekani. Inertial squirmer. *Physics of Fluids*, 24(10), 2012.

Supporting Information: Swimming mode determines how well mesoscale swimmers shield their odor in turbulence

I. MODELING SWIMMER DYNAMICS

As noted in the main text, swimmers are modeled as force dipoles oriented along the streamwise direction, represented as $F(\delta(\mathbf{x} + \mathbf{r}) - \delta(\mathbf{x} - \mathbf{r}))\hat{\mathbf{x}}$. The magnitude of F is computed according to

$$F = C_D \rho A u_s^2 / 2. \quad (\text{S1})$$

where C_D is the drag coefficient, ρ is the density of the fluid, A is the projected area of the swimmer and u_s is the swimmer speed [28]. Following ref. [28], the values of the drag coefficient are given by

$$C_D = \frac{24}{Re_s} (1 + 0.1315 Re_s^{(0.82 - 0.05 \log_{10} Re_s)})$$

for $Re_s = 10$ and

$$C_D = \frac{24}{Re_s} (1 + 0.1935 Re_s^{0.6305})$$

for $Re_s = 25$ and 50. After an initial simulation, the value of F is further adapted to account for the change in local fluid velocity due to the dynamics of pusher-like and puller-like swimmers.

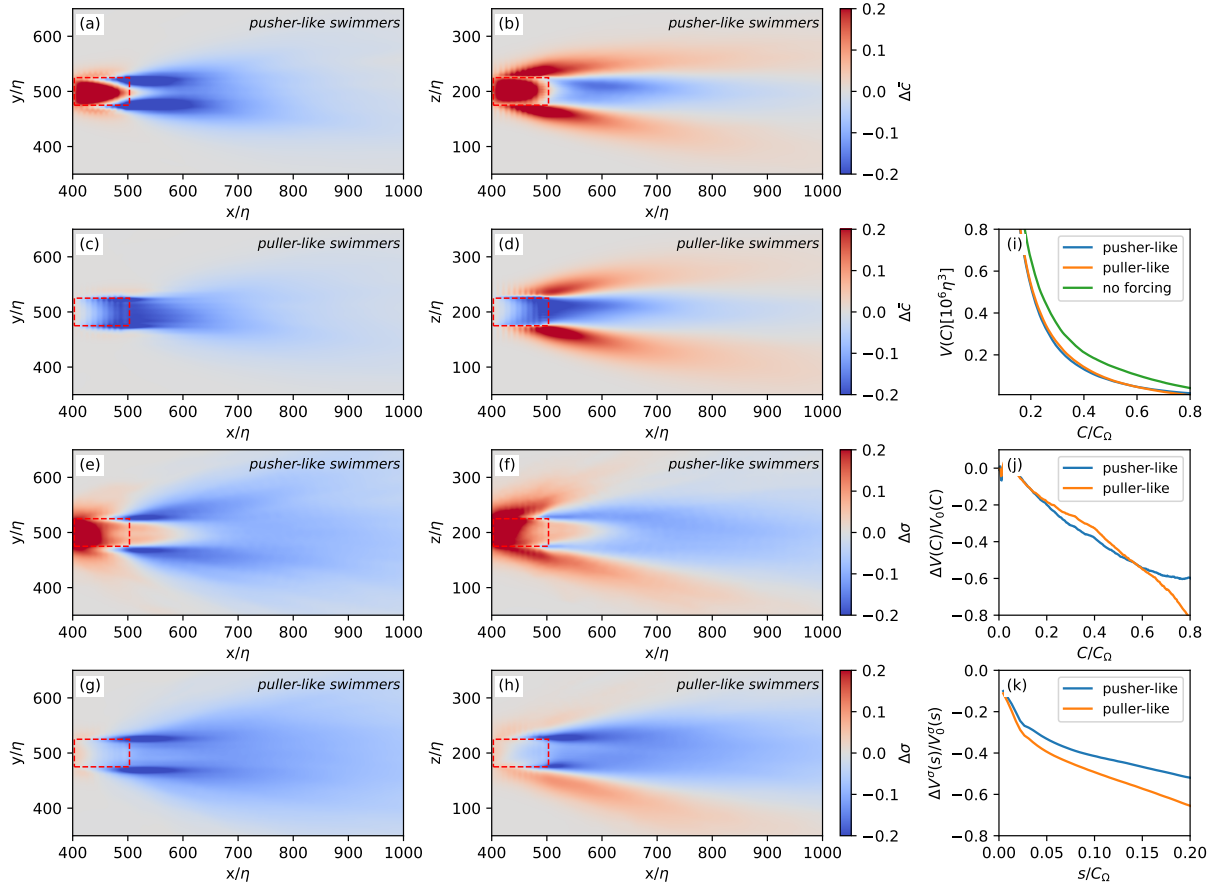


FIG. S1. Statistics of the mean odor field when the swimmers are arranged in a box of same width to height aspect ratio. (a) Horizontal and (b) vertical cross-sections of the mean odor field for differential $\Delta \bar{c}(\mathbf{x})$ for pusher-like swimmers. Panels (c) and (d) show the same for puller-like swimmers. Horizontal and vertical cross-sections of the odor standard deviation differential $\Delta \sigma(\mathbf{x})$ for (e,f) pusher-like and (g,h) puller-like swimmers. (i) Volume $V(C)$ for both types of swimmers and for the baseline case. (j) The corresponding shielding intensities $\Delta V(C)/V_0(C)$. (k) Shielding intensity of the odor fluctuations $\Delta V_\sigma(s)/V_{\sigma_0}(s)$.

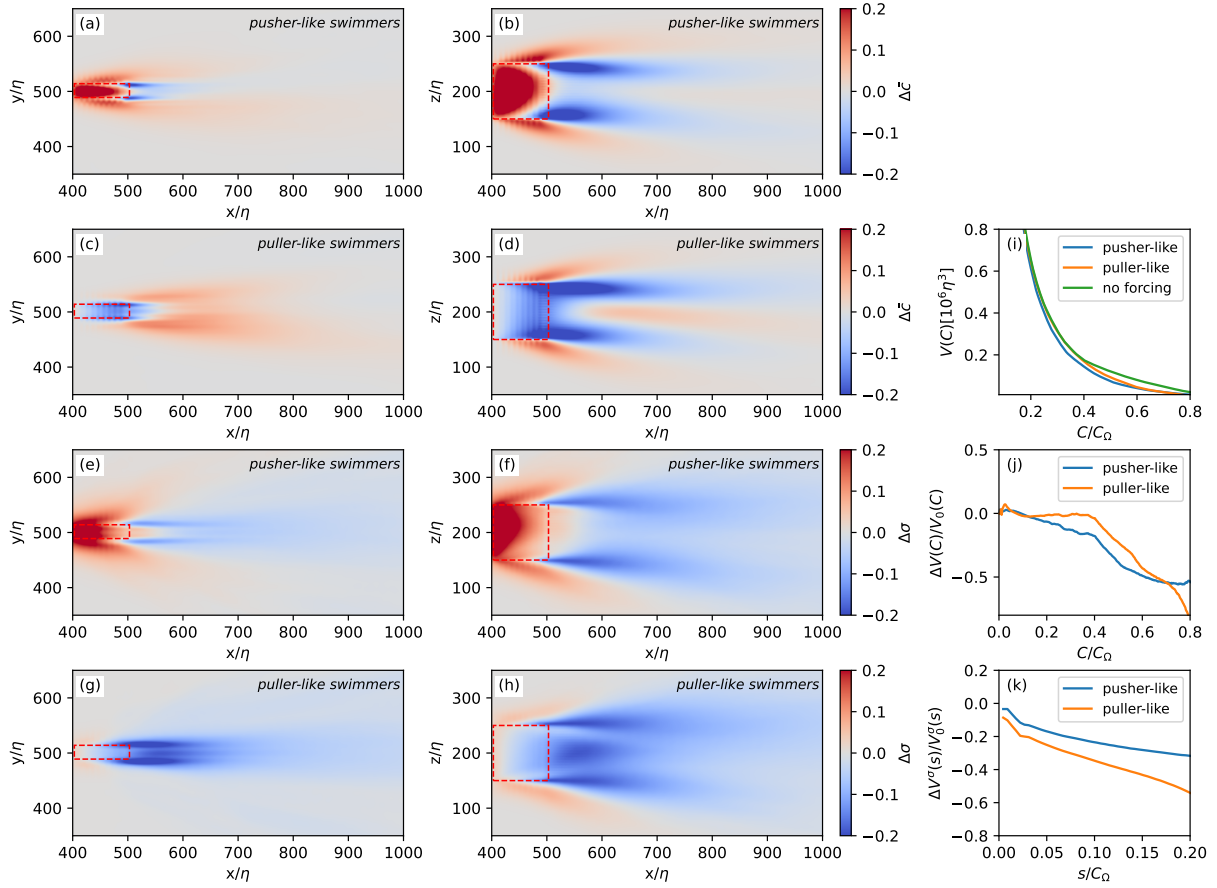


FIG. S2. Statistics of the mean odor field when the swimmers are arranged in a box different aspect ratio than those presented in the main text. (a) Horizontal and (b) vertical cross-sections of the mean odor field for differential $\Delta \bar{c}(\mathbf{x})$ for pusher-like swimmers. Panels (c) and (d) show the same for puller-like swimmers. Horizontal and vertical cross-sections of the odor standard deviation differential $\Delta \sigma(\mathbf{x})$ for (e,f) pusher-like and (g,h) puller-like swimmers. (i) Volume $V(C)$ for both types of swimmers and for the baseline case. (j) The corresponding shielding intensities $\Delta V(C)/V_0(C)$. (k) Shielding intensity of the odor fluctuations $\Delta V_\sigma(s)/V_{\sigma 0}(s)$.

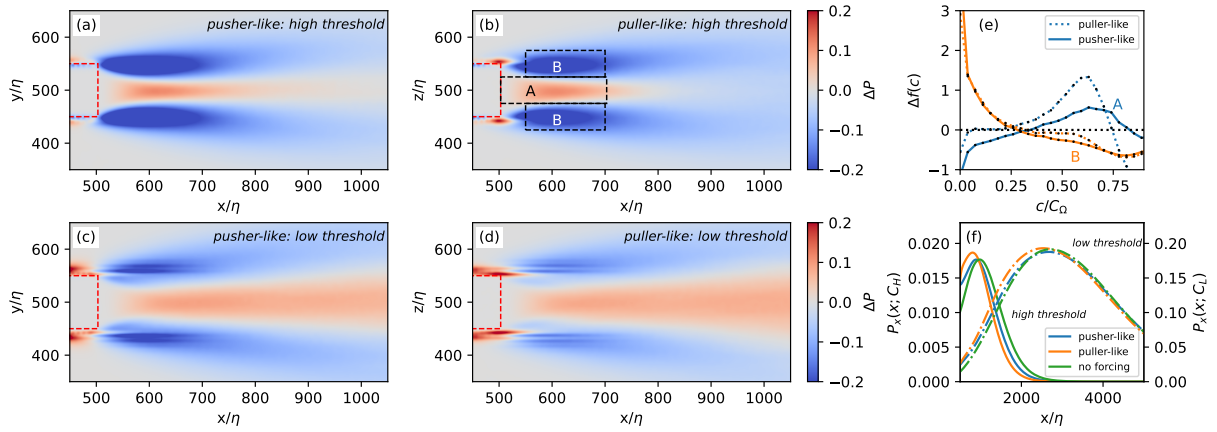


FIG. S3. The detection probability differential $\Delta P(\mathbf{x}; C_H)$ at a high threshold (C_H) for (a) pusher-like and (b) puller-like swimmers. $\Delta P(\mathbf{x}; C_L)$ at a low threshold (C_L) for (c) pusher-like and (d) puller-like swimmers. (e) Odor pdf differential $\Delta f(c; \Omega_{A/B})$ for pusher-like and puller-like swimmers showing that the hydrodynamic fluctuations due to the swimming dynamics result in an effective eddy diffusivity. (f) Gross detection probability $P_x(x; C)$ as a function of stream-wise direction for both low and high detection thresholds showing that at large distances, the detection probability is damped due to the swimming dynamics.

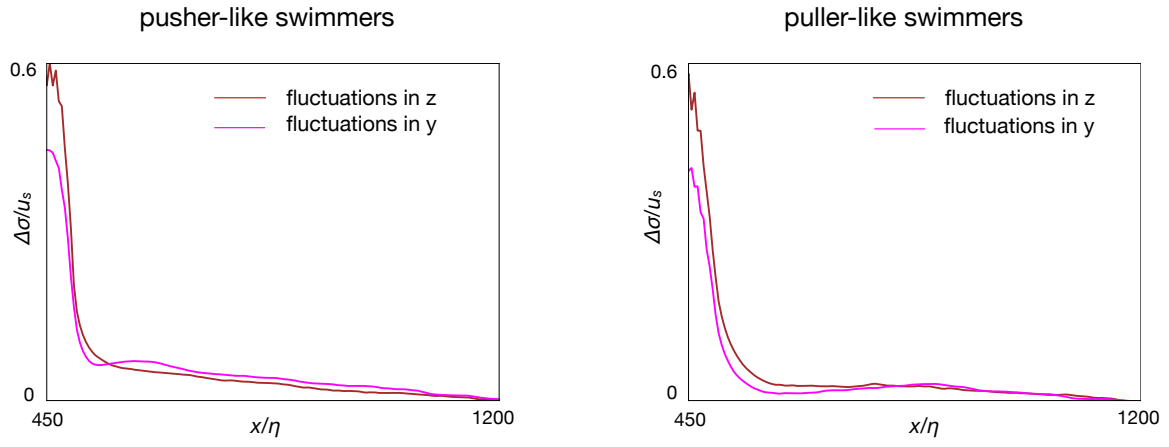


FIG. S4. Differences in the standard deviation of the velocity fluctuations in the wall-normal and span-wise directions for pusher-like and puller-like swimmers.